Photodissociation of $[Fe_x(C_{24}H_{12})_y]^+$ Complexes in the PIRENEA Setup: Iron-Polycyclic Aromatic Hydrocarbon Clusters as Candidates for Very Small Interstellar Grains

Aude Simon* and Christine Joblin

Université de Toulouse, UPS, CESR, 9 av. du colonel Roche F-31028 Toulouse Cedex 09, France, and CNRS, UMR5187, F-31028 Toulouse, France

Received: November 12, 2008; Revised Manuscript Received: January 28, 2009

Astronomical observations suggest that polycyclic aromatic hydrocarbons (PAHs) that emit at the surface of molecular clouds in the interstellar medium are locally produced by photodestruction of very small grains (VSGs). In this paper, we investigate $[Fe_x(PAH)_y]^+$ clusters as candidates for these VSGs. $[FeC_{24}H_{12}]^+$ and $[Fe_x(C_{24}H_{12})_2]^+$ ($x = 1-3$) complexes were formed by laser ablation of a solid target in the PIRENEA setup, a cold ion trap dedicated to astrochemistry. Their photodissociation was studied under continuous visible irradiation. Photodissociation pathways are identified and characteristic time scales for photostability are provided. $[Fe_x(C_{24}H_{12})_2]^+$ ($x = 1-3$) complexes sequentially photodissociate by losing iron atoms and coronene units under laboratory irradiation conditions with $C_{24}H_{12}^+$ as the smallest photofragment. The study of the dissociation kinetics gives interesting insights into the structures of the complexes. The dissociation rate is found to increase with the complex size. Density functional theory (DFT) and time-dependent DFT calculations show that the increase of the number of Fe atoms leads to an increased stability of the complex but also to an increased heating rate in the experimental conditions, due to the presence of strong electronic excitations in the visible. The modeling of the dissociation kinetics of the smallest complex $[FeC_{24}H_{12}]^+$ by using a kinetic Monte Carlo code allows derivation of the dissociation parameters and the internal energy for this complex, showing in particular that it could dissociate under interstellar irradiation conditions. First insights into the dissociation of larger complexes in these conditions are also given.

Introduction

Polycyclic aromatic hydrocarbons (PAHs) and PAH-related molecules have been proposed as the carriers of the family of the aromatic infrared bands (AIBs) observed in many astronomical objects.[1,2] Since then, there have been several studies to understand the formation and processing of PAHs in the circumstellar environment of evolved stars[3−8] and their further processing by shocks in the diffuse interstellar medicum (ISM)[9] where they are injected before being incorporated into molecular clouds. Studies of the IR emission of molecular clouds point to the fact that the carriers of the mid-IR emission are present only at the cloud surface that is exposed to UV radiation.[10,11] Recent analysis of spectro-imagery data strongly suggests that the carriers of the AIBs are indeed produced there by photodestruction of very small grains (VSGs).[12,13] This process is observed at rather low UV flux and is expected to affect the VSGs that are small enough to undergo significant temperature fluctuations (typical radius less than 20 Å).[28] Furthermore, if the photodestruction is thermally driven, these VSGs are expected to be loosely bonded. Candidates for these VSGs are PAH clusters that could form by aggregation of PAH units in the denser and UV-shielded part of the clouds.[15,16] The model by Marty et al.[17] predicts that this aggregation also involves heavy atoms and in particular iron. This therefore motivates studies on the properties of both PAH clusters and mixed aggregates of PAHs and Fe atoms. Serra et al.[18] and Chaudret et al.[19] first proposed that Fe-PAH π-adducts are stable species that can form efficiently in the conditions of the ISM and play a role in its chemistry. Following this proposal, some astronomical modeling[17] showed that organometallic complexes made of PAHs and iron can form and survive in molecular clouds in regions with sufficient shielding from UV photons. This model takes into account the formation and photodissociation reactions of these complexes. However, it suffers from the lack of experimental and reliable theoretical data concerning coordination complexes between PAHs and transition metals.

The relevance of Fe-PAH complexes in astrochemistry remains a controversial issue in the community of astrophysicists despite some observational evidence for their presence. Several authors suggested that part of the iron and other heavy elements are in the form of atoms that attach and desorb from very small carbonaceous grains.[18,20−24] Measurements of the gas-phase abundances of Fe (and Si) in translucent sight lines show that more of these elements are in the dust phase when the nonlinear far-UV rise of the extinction curve increases.[25] By consideration that this rise can be entirely accounted for by PAHs and related VSG species,[26] this supports the role of the latter species in the depletion of Fe (and Si) from the gas phase.

Motivated by the astrophysical context, the first experimental study on the formation and photodissociation of $[FePAH]^+$ and $[Fe(PAH)_2]^+$ complexes was published,[27] under the collision-free conditions of an ion cyclotron resonance (ICR) mass spectrometer. This study was performed for a small PAH (naphthalene $C_{10}H_8$), for which high-enough vapor pressure can be easily obtained. The formation of $[FePAH]^+$ and $[Fe(PAH)_2]^+$ by radiative association was shown to be fast and that of $[Fe(PAH)_2]^+$ to proceed through a two-step accretion rather than a three-body reaction. The barrier to dissociation of $[Fe(C_{10}H_8)_2]^+$ was measured between 1 and 2 eV. Experimental and theoretical infrared spectra of $[FePAH]^+$ and $[Fe(PAH)_2]^+$

* To whom correspondence should be addressed. E-mail: aude.simon@cesr.fr.

10.1021/jp8099785 CCC: $40.75
Published on Web 04/01/2009

for naphthalene $C_{10}H_8$ and fluorene $C_{13}H_{10}$ in the gas phase were reported recently.[28] Experimental studies on organometallic complexes involving larger PAHs, which are likely to be more astrophysically relevant, are scarce due to the difficulties triggered by their low vapor pressure. The fast formation of $[FeC_{24}H_{12}]^+$ and $[Fe(C_{24}H_{12})_2]^+$ by radiative association in an ICR cell was shown by Pozniac and Dunbar.[29] Iron corannulene $[FeC_{20}H_{10}]^+$ and iron coronene $[FeC_{24}H_{12}]^+$ adduct ions were formed in the selected-ion flow tube (SIFT) apparatus in Bohme's group by attaching Fe^+ to the respective aromatic molecule in a flowing He bath gas, and their reactivity with small molecules was studied.[30,31] The production of $[(TM)_xPAH_y]^+$ complexes (TM = transition metal) by laser ablation of a mixture of metal powder, metal oxide, or other materials with the PAH of interest was shown not to be efficient, especially in the case of iron.[32] The formation of $[(TM)_x(PAH)_y]^{\pm}$ complexes in the gas phase has been achieved with the development of laser vaporization cluster sources.[32−37] Cationic complexes of pyrene $C_{16}H_{10}$ and coronene $C_{24}H_{12}$ with niobium,[36] chromium,[34] and iron[33,38] were characterized by means of laser photodissociation experiments.[33,34,36,38] Anionic complexes with titanium, vanadium,[35] and iron[37] were formed and characterized by photoelectron spectroscopy. The experiments on $[Fe_x(C_{24}H_{12})_y]^{\pm}$ were complemented by density functional theory (DFT) calculations[39,37] to gain insights into their geometric and electronic structures. Although this interplay between DFT calculations and mass spectrometry experiments appears as the best approach to improve our knowledge on such complex systems as $[(TM)_x(PAH)_y]^{\pm}$, many uncertainties remain. For instance, the comparison between experimental infrared multiple photodissociation (IRMPD) spectra and calculated IR absorption spectra has not allowed to unambiguously assign an electronic state for $[XFeC_{24}H_{12}]^+$ complexes (X = C_5H_5 or Cp, $C_5(CH_3)_5$ or Cp*).[40]

The theoretical characterization of the structures and thermodynamics of iron-PAH, and in general transition metal-PAH complexes, is known to be challenging. The size of these systems and their large density of electronic states and structures inherent to organometallic unsaturated species make the determination of their electronic and geometric structures difficult. A few theoretical papers have been published.[39,41−43] For complexes with several metal atoms, the structures of $([Fe_2C_{24}H_{12}]^{+/0})$,[39] $[Fe_m(C_{24}H_{12})_n]^-$ (m = 1, 2, n = 1, 2),[37] and $([Fe_7C_{24}H_{12}]^0)$[42] were investigated. These studies were essentially motivated by the magnetic properties of complexes of transition metals with PAHs. In the first theoretical paper by our group,[43] we provided thermodynamic data and showed that $FePAH^+$ complexes are more stable than their neutral counterparts. The major effect of the coordination of Fe on a PAH^+ on the IR spectrum was shown to be a global decrease of the intensity in the [6−10 μm] region. This was confirmed by IRMPD experiments on $[XFeC_{24}H_{12}]^+$ model complexes (X = Cp, Cp*).[40]

This paper reports new experimental results on the photoevaporation of $[Fe_x(C_{24}H_{12})_y]^+$ complexes produced in the PIRENEA setup, which has been specifically developed for astrochemistry.[44] The photodissociation pathways and kinetics of the $[Fe_x(C_{24}H_{12})_y]^+$ (x,y) =((1,1) or (1−3, 2)) complexes are presented in section 3.1. In section 3.2, we show how these results can be used to gain insight into the structures of the $[Fe_x(C_{24}H_{12})_y]^+$ complexes. The interpretation of the observed experimental trends is guided by ground- and excited-state electronic structure calculations. Finally, in section 3.3, the measured photodissociation kinetics for $[FeC_{24}H_{12}]^+$ is simulated by a kinetic Monte Carlo code to quantify the dissociation parameters. First astrophysical implications are given.

Methods

Experimental Methods. The PIRENEA experimental setup combines the electromagnetic trapping and the mass spectrometry performances of an ICR cell with cryogenic cooling. It has been first described by Joblin et al.[44] Ions are formed by laser ablation of a solid target using a Nd:YAG laser at 266 nm. The target is located out of the magnet, but some ions manage to reach the opened cyclindrical ICR cell where they are dynamically trapped by means of electrostatic potentials. The pressure in the chamber remains below 10^{-10} mbar, and the temperature of the cell is ∼30 K thanks to the cryogenic cooling. In an ICR spectrometer, the ion signal that is used for mass analysis is generated by exciting coherently the ion cloud with an alternating electric field. The ion motion induces an image charge signal on the detection electrodes and this transient signal is recorded and analyzed by Fourier Transform (FT) to retrieve the mass-overcharge ratio (m/z).[45] The experimental procedure consists in production and isolation of the ions of interest, irradiation with the light source, and mass analysis. If several species are present in the ICR cell after laser ablation, those of interest at a given m/z ratio can be isolated by selective ejection of all the other species.[46] The remaining isolated ions are then irradiated by the continuous UV−visible light emitted by a Xenon arc lamp in the [200−800] nm range. The wavelength range can be adjusted by using long-pass color filters. The cutoff wavelength is defined at 50% of transmission. In the present experiments, we used the 475-nm filter. The dissociation kinetics is given by the relative abundances of the parent ion and its photofragments as a function of the irradiation time which varies from hundreds of milliseconds to several seconds.

Computational. As it will be shown in next section, the experimental results presented in this paper give interesting insights into the thermodynamics and structures of $[Fe_x(C_{24}H_{12})_2]^+$ complexes (x = 1−3), which are difficult to study theoretically as emphasized above. To complete these results, DFT calculations were performed to obtain thermodynamic data for $[FeC_{24}H_{12}]^+$, $[Fe(C_{24}H_{12})_2]^+$, and $[Fe_2(C_{24}H_{12})_2]^+$. Geometry optimizations and frequency calculations were done at the BPW91[47,48]/Lanl2DZ[49] level of theory. The BPW91 hybrid functional was recently used by Li et al.[37] to obtain the geometries and electronic structures of $[Fe_m(C_{24}H_{12})_n]^-$ (m = 1, 2, n = 1, 2). It was also shown to be the most appropriate functional for the description of the electronic structures of iron clusters.[50,51] The Lanl2DZ basis set was chosen for a first survey of the potential energy surfaces (PES) because of its very low computational cost. Thermodynamic data were estimated by single point calculations of the electronic energies at the MPW1PW91[52]/6-31+G(d,p) level for the geometries optimized at the BPW91/Lanl2DZ level. For the largest complex $[Fe_2(C_{24}H_{12})_2]^+$, the PES was first investigated using the DFT-based tight binding (DFTB) method[53−55] implemented in the DeMon code.[56] DFTB is a semiempirical method derived from the DFT and developed to treat extended systems by allowing a very fast exploration of the PES with respect to DFT. The most stable geometry obtained at the DFTB level was then reoptimized at the BPW91/Lanl2dz level. All the calculated structures presented in this paper were found as minima at this level. To describe the photophysics of the irradiated species in the PIRENEA setup, the electronic spectra of $[FeC_{24}H_{12}]^+$, $[Fe(C_{24}H_{12})_2]^+$, and $[Fe_2(C_{24}H_{12})_2]^+$ were estimated using time-dependent DFT calculations (TD-DFT)[57] at the BPW91/

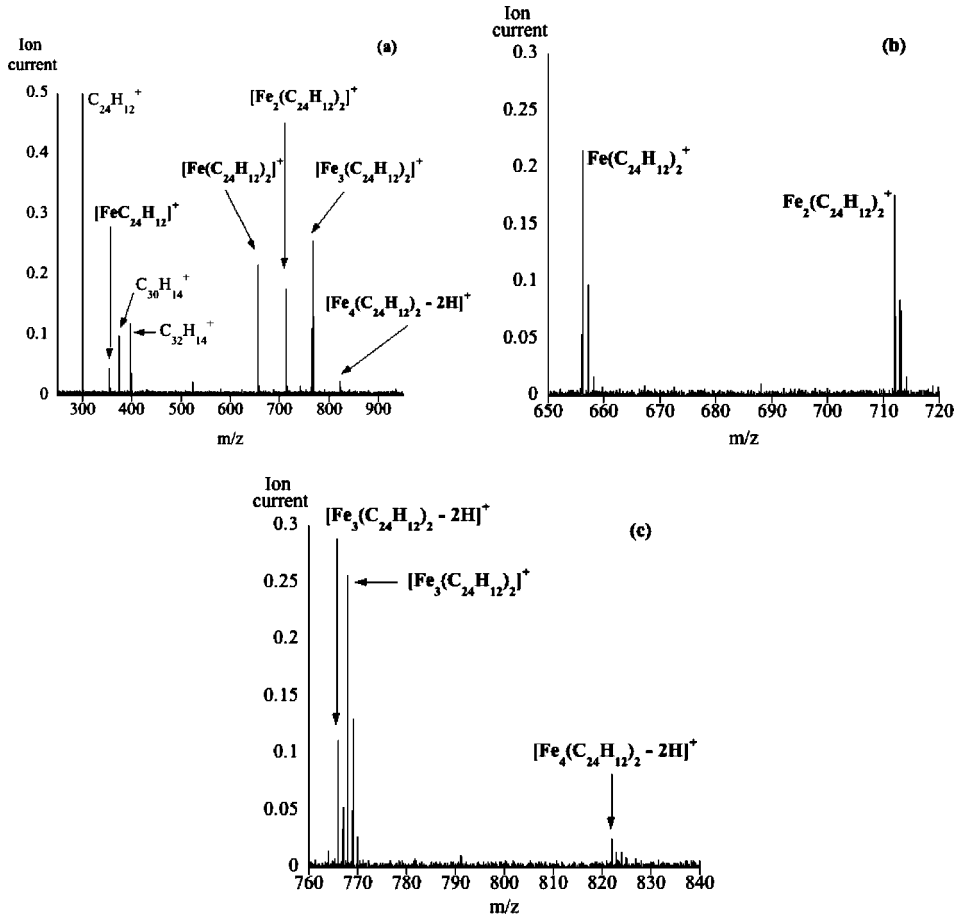

Figure 1. (a) Mass spectrum recorded after laser ablation of the $[Fe_3(CO)_{12} + C_{24}H_{12}]$ solid target in the PIRENEA setup. (b and c) Details of the mass spectrum in the [650−720] *m/z* and [760−840] *m/z* range, respectively.

Lanl2DZ level. All DFT and TD-DFT calculations were performed using the Gaussian 03 suite of programs.[58]

Results and Discussion

Photoevaporation of $[Fe_x(C_{24}H_{12})_y]^+$ Complexes in the PIRENEA Setup. $[Fe_x(C_{24}H_{12})_y]^+$ species were produced by laser ablation of a solid target made of a mixture of triiron-dodecacarbonyl $[Fe_3(CO)_{12}]$ and coronene $C_{24}H_{12}$ (Sigma-Aldrich, St Quentin Fallavier, France) deposited onto a thin layer of silica nanoparticles.[59]

The mass spectrum recorded 2 s after laser ablation is reported in Figure 1a. Details of this spectrum in the [650−720] and [760−840] *m/z* range are reported in parts b and c of Figure 1, respectively. Three major peaks corresponding to $[Fe(C_{24}H_{12})_2]^+$ ($m/z = 656$), $[Fe_2(C_{24}H_{12})_2]^+$ ($m/z = 712$), and $[Fe_3(C_{24}H_{12})_2]^+$ ($m/z = 768$) are observed, and their isotopic patterns can be clearly distinguished. Smaller peaks are assigned to $[FeC_{24}H_{12}]^+$ ($m/z = 356$) and $[Fe_4(C_{24}H_{12})_2\text{-}2H]^+$ ($m/z = 822$). As can be seen in Figure 1c, dehydrogenated species start to be observed for complexes with at least three iron atoms, and their relative abundances with respect to the fully hydrogenated ones seem to increase with the number of iron atoms. The peaks located at $m/z = 300$, 374, and 398 correspond to the PAH species $C_{24}H_{12}^+$, $C_{30}H_{14}^+$, and $C_{32}H_{14}^+$, respectively, that are also observed in laser ablation of pure $C_{24}H_{12}$. Interestingly, the $[Fe_x(C_{24}H_{12})_y]^+$ complexes $(x,y) = (1,1)$ and $(1-3,2)$ were formed in a cluster source[33] along with other clusters containing three coronene molecules and complexes with one coronene molecule and up to three Fe atoms. The low mass-resolution of the experiment did not however allow the authors to identify the presence of dehydrogenated species.

Each $[Fe_x(C_{24}H_{12})_y]^+$ complex $(x,y) = (1,1)$ and $(1-3,2)$ was mass selected in our experiment and irradiated by the continuous light of the Xenon arc lamp available on the PIRENEA setup. A long-pass filter with cutoff at 475 nm was used in order to decrease the photodissociation rate. For instance, 50% of the $[Fe(C_{24}H_{12})_2]^+$ ions were already dissociated after 120 ms of irradiation without filter. This time scale is too short to study the dissociation kinetics considering the precision of the lamp shutter opening (∼50 ms). The same irradiation conditions were used for all complexes.

As can be seen in Figure 2, only one photofragment $C_{24}H_{12}^+$ is observed for $[FeC_{24}H_{12}]^+$. The loss of one Fe atom was expected as it was shown to be the lowest energy pathway using DFT calculations.[43] The same channel was observed under irradiation with a 532 or 355 nm laser.[33] The evolution of the normalized intensities of $[FeC_{24}H_{12}]^+$ and $C_{24}H_{12}^+$ as a function of the irradiation time is reported in Figure 3, and a characteristic time τ_1 for dissociation was extracted (cf. Table 1) according to

$$I_{\text{parents}} = I_0 \exp(-t/\tau_1) \quad (1)$$

$$I_{\text{fragments}} = I_0(1 - \exp(-t/\tau_1)) \quad (2)$$

In the case of $[Fe(C_{24}H_{12})_2]^+$, two major photofragments $[FeC_{24}H_{12}]^+$ and $C_{24}H_{12}^+$ are formed (cf. Figure 4). These results

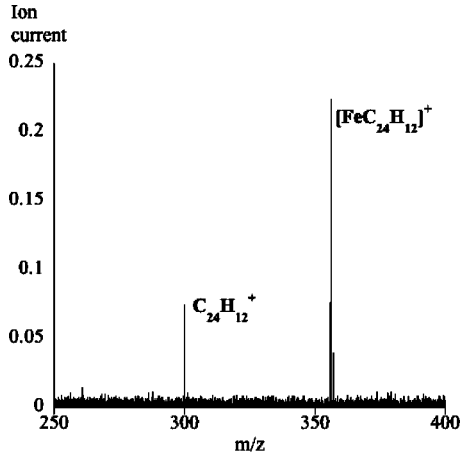

Figure 2. Mass spectrum recorded after 700 ms irradiation of mass selected $[FeC_{24}H_{12}]^+$ ions using a xenon arc lamp and a 475-nm long-pass filter.

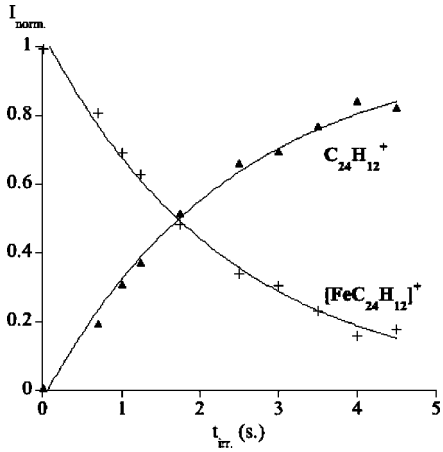

Figure 3. Normalized intensities of the $[FeC_{24}H_{12}]^+$ parent ion (crosses) and its photofragment $C_{24}H_{12}^+$ (full triangles) as a function of irradiation time (Xe arc lamp, 475-nm long-pass filter). Experimental points are fitted assuming first order kinetics (cf. eqs 1 and 2).

TABLE 1: Characteristic Dissociation Times τ Obtained by the Fit of the Normalized Experimental Intensities (cf. Equations 1 and 2) and Values of τ_{eq} Derived from Equation 6 or Directly from the Experimental Curves

species	τ (s)	τ_{eq} (s) (eq 6)	τ_{eq} (s) (exptl)
$[FeC_{24}H_{12}]^+$	$\tau_1 = 2.38 \pm 0.04$		
$[Fe(C_{24}H_{12})_2]^+$	$\tau_2 = 1.83 \pm 0.04$	2.1 ± 0.1	2.0 ± 0.2
$[Fe_2(C_{24}H_{12})_2]^+$	$\tau_3 = 0.63 \pm 0.04$	1.1 ± 0.2	0.8 ± 0.1
$[Fe_3(C_{24}H_{12})_2]^+$	$\tau_4 = 0.54 \pm 0.02$	0.1 ± 0.1	0.4 ± 0.2

are different from the ones obtained by Buchanan et al.[33] who mentionned they only observed the $C_{24}H_{12}^+$ photofragment after irradiation of $[Fe(C_{24}H_{12})_2]^+$ with a 355 or 532 nm laser. A plausible explanation is that the irradiation conditions were more severe in these laser experiments and therefore prevented the observation of the primary fragment ion $[FeC_{24}H_{12}]^+$. The normalized intensities of the $[Fe(C_{24}H_{12})_2]^+$ parent ion and its photofragments as a function of the irradiation time are reported in Figure 5. The evolution of the relative abundances of $[FeC_{24}H_{12}]^+$ and $C_{24}H_{12}^+$ illustrates the sequential character of the photodissociation. It can be quantified using the following equation scheme

$$[Fe(C_{24}H_{12})_2]^+ \rightarrow [FeC_{24}H_{12}]^+ + C_{24}H_{12} \quad \left(k_2 = \frac{1}{\tau_2}\right) \quad (3)$$

$$[FeC_{24}H_{12}]^+ \rightarrow C_{24}H_{12}^+ + Fe \quad \left(k_1 = \frac{1}{\tau_1}\right) \quad (4)$$

One thus obtains

$$I_{norm-[FeC_{24}H_{12}]^+} = \frac{\tau_1}{\tau_2 - \tau_1}[\exp(-t/\tau_2) - \exp(-t/\tau_1)] \quad (5)$$

The time τ_{eq} at which $I_{norm-[FeC_{24}H_{12}]^+}$ reaches its maximum is obtained for $(dI_{norm-[FeC_{24}H_{12}]^+})/(dt)$ is equal to 0, leading to

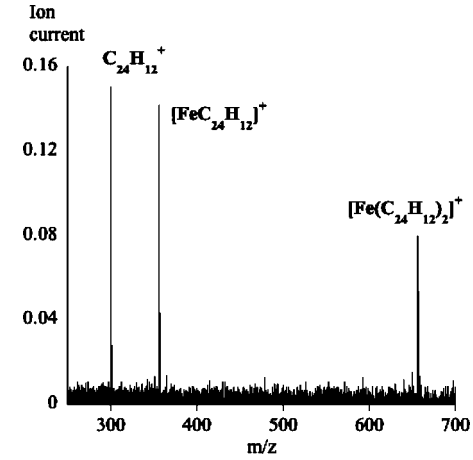

Figure 4. Mass spectrum recorded after 2 s of irradiation of mass-selected $[Fe(C_{24}H_{12})_2]^+$ ions with a xenon arc lamp and a 475-nm long-pass filter.

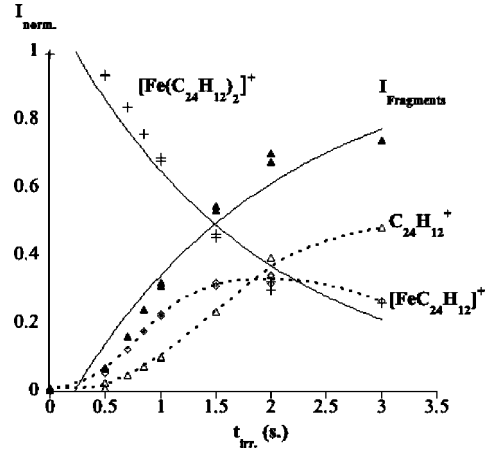

Figure 5. Normalized intensities of the $[Fe(C_{24}H_{12})_2]^+$ parent ions (crosses), all photofragments (full triangles), and each individual photofragment ($[FeC_{24}H_{12}]^+$ (purple open diamonds) and $C_{24}H_{12}^+$ (blue open triangles) as a function of irradiation time (Xe arc lamp, 475-nm long-pass filter). Experimental points for the parent and global fragment intensities are fitted according to eqs 1 and 2. The dashed lines were drawn to facilitate the reading.

$$\tau_{eq} = \frac{\tau_1\tau_2}{\tau_1 - \tau_2}\ln\left(\frac{\tau_1}{\tau_2}\right) \quad (6)$$

For the intermediate species $[FeC_{24}H_{12}]^+$ in the photodissociation of $[Fe(C_{24}H_{12})_2]^+$, a τ_{eq} value of 2.1 ± 0.1 s was obtained with $\tau_1 = 2.38$ s and $\tau_2 = 1.83$ s (cf. Table 1). This is in agreement with the value directly derived from the experimental points (cf. Figure 5). This result strongly supports that the sequential mechanism as given by eqs 3 and 4 is valid.

At short irradiation time, the observed fragmentation rate appears to be below the curves given by eqs 1 and 2. This could be explained by the fact that the effective irradiation time is shorter than the time of the lamp shutter opening by typically 50 ms. More likely, this is related to the experimental dissociation conditions. As described in Boissel et al.,[60] continuous irradiation with the Xe lamp leads to the building of the internal energy U in PAHs due to the efficient internal conversion (IC) process which converts electronic energy into vibrational energy in the ground state. Dissociation then proceeds for the species with the highest values of U attained by multiple photon absorption, which takes some time. We make here the reasonable asumption that the IC process is also very efficient for $[Fe_x(C_{24}H_{12})_y]^+$ complexes. At short irradiation times, the distribution of U has not attained its equilibrium yet. The dissociation rate, which depends steeply on the highest values of U, is therefore expected to be slower (cf. Figure 4 in Boissel et al.).[60] In the simulations described in section 3.3 for the $[FeC_{24}H_{12}]^+$ complex, we found that a time of ~500 ms is required to reach equilibrium.

The results for the photodissociation of $[Fe_2(C_{24}H_{12})_2]^+$ are shown in Figure 6 and Figure 7, the only photofragment observed at short irradiation times is $[Fe(C_{24}H_{12})_2]^+$, resulting from the detachment of one Fe atom.

$$[Fe_2(C_{24}H_{12})_2]^+ \rightarrow [Fe(C_{24}H_{12})_2]^+ + Fe \qquad \left(k_3 = \frac{1}{\tau_3}\right) \quad (7)$$

The photodissociation rate of $[Fe_2(C_{24}H_{12})_2]^+$ ($\tau_3 = 0.63 \pm 0.04$ s, cf. Table 1) was found to be approximatively three times faster than that of $[FeC_{24}H_{12}]^+$ and twice as fast as that of $[Fe(C_{24}H_{12})_2]^+$. Considering the photodissociation patterns reported in Figure 7 and our knowledge on the photodissociation of $[Fe(C_{24}H_{12})_2]^+$ and $[FeC_{24}H_{12}]^+$ (eqs 3 and 4), we derived a τ_{eq} value for the largest photofragment $[Fe(C_{24}H_{12})_2]^+$ of 1.1 ± 0.2 s (using eq 6 with τ_3 and τ_4 instead of τ_1 and τ_2) in agreement with the value that can be read in Figure 7 ($(dI_{norm-[Fe(C_{24}H_{12})_2]^+})/(dt) = 0$ at 0.8 ± 0.1s).

The study of the $[Fe_3(C_{24}H_{12})_2]^+$ ion was the most delicate as a significant amount of dehydrogenated species $[Fe_3(C_{24}H_{12})_2\text{-}2H]^+$ was formed during the laser ablation prior to irradiation. As can be seen in the left spectrum of Figure 8, the $[Fe_2(C_{24}H_{12})_2]^+$ photofragment resulting from the detachement of one iron atom appears at short irradiation time. For irradiation times longer than 500 ms, the spectrum becomes complicated as not only the $[Fe(C_{24}H_{12})_2]^+$, $[FeC_{24}H_{12}]^+$, and $[C_{24}H_{12}]^+$ ions are observed but also $[Fe(C_{24}H_{12})_2\text{-}6H]^+$, $[Fe_3C_{24}H_{12}]^+$, and $[Fe_2C_{24}H_{12}]^+$ (cf. Figure 8, bottom spectrum). The presence of these ions shows the occurrence of other dissociation channels, possibly associated to different isomers. It is however not possible to say if these isomers are present in the cell before irradiation or if they are formed by rearrangement during the heating process. Because of the complexity of these patterns, the presence of these ions has not been taken into account in the kinetic study that follows. The normalized intensities of the fragment ions, i.e., $[Fe_2(C_{24}H_{12})_2]^+$, $[Fe(C_{24}H_{12})_2]^+$, $[FeC_{24}H_{12}]^+$, and $[C_{24}H_{12}]^+$, as a function of the irradiation time are reported in Figure 9. A characteristic time τ_4 slightly lower than that of $[Fe_2(C_{24}H_{12})_2]^+$ is derived (cf. Table 1). By consideration of the photodissociation patterns reported in Figure 9 and our knowledge on the photodissociation of $[Fe_2(C_{24}H_{12})_2]^+$, $[Fe(C_{24}H_{12})_2]^+$, and $[FeC_{24}H_{12}]^+$, we can conclude on a sequential photodissociation pattern as summarized in Figure 10. We extracted a τ_{eq} value of 0.1 ± 0.1 s for the primary photofragment $[Fe_2(C_{24}H_{12})_2]^+$, in line with the value extracted from the experimental data ($(dI_{norm - [Fe_2(C_{24}H_{12})_2]^+})/(dt) = 0$ at 0.4 ± 0.2s). These results are reported in Table 1 and Figure 9.

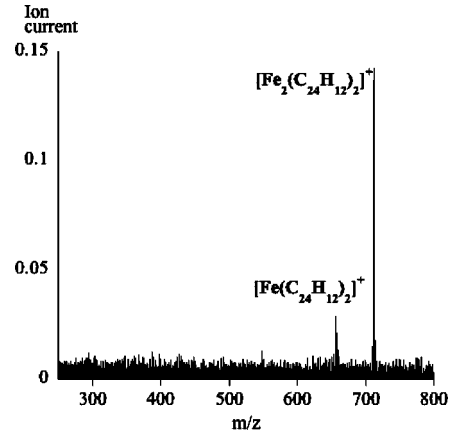

Figure 6. Mass spectrum recorded after 200 ms irradiation of mass-selected $[Fe_2(C_{24}H_{12})_2]^+$ ions with a xenon arc lamp and a 475-nm long-pass filter.

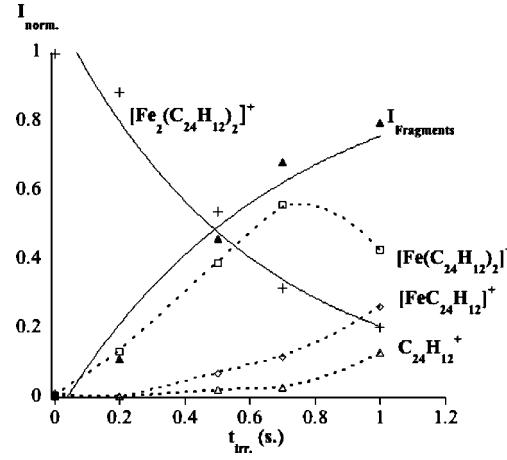

Figure 7. Normalized intensities of the $[Fe_2(C_{24}H_{12})_2]^+$ parent ions (crosses), all photofragments (full triangles), and each individual photofragment $[Fe(C_{24}H_{12})_2]^+$ (open squares), $[FeC_{24}H_{12}]^+$ (open diamonds), and $C_{24}H_{12}^+$ (open triangles)) as a function of irradiation time (Xe arc lamp, 475-nm long-pass filter). Experimental points for the parent and global fragment intensities are fitted according to eqs 1 and 2. The dashed lines were drawn to facilitate the reading.

Structures, Thermochemistry, and Photoabsorption Efficiency. The photodissociation pathways and kinetics give interesting insights into the structures and thermodynamics of the complexes. In the previous section, we have shown that the products and characteristic time scales of dissociation are similar for a complex of a given *m/z* ratio formed either by laser ablation or by photodissociation of larger precursors. This suggests that only the most thermodynamically stable species have been

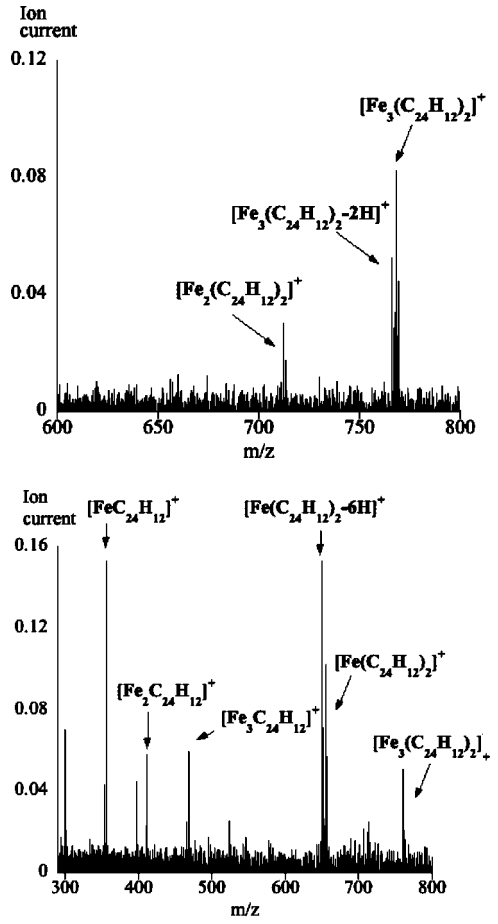

Figure 8. Mass spectra recorded after irradiation of mass-selected $[Fe_3(C_{24}H_{12})_2]^+$ and $[Fe_3(C_{24}H_{12})_2\text{-}2H]^+$ ions with a xenon arc lamp and a 475-nm long-pass filter. (Top and bottom spectra: 200 ms and 1 s irradiation, respectively.)

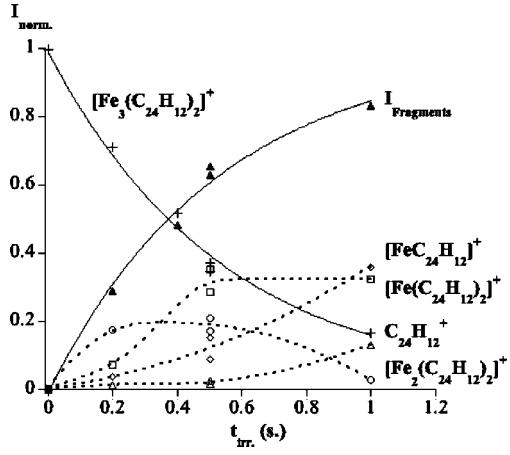

Figure 9. Normalized intensities of the $[Fe_3(C_{24}H_{12})_2]^+$ parent ions (crosses), all photofragments (full triangles), and each individual photofragment ($[Fe_2(C_{24}H_{12})_2]^+$ (open dots), $[Fe(C_{24}H_{12})_2]^+$ (open squares), $[FeC_{24}H_{12}]^+$ (open diamonds), and $C_{24}H_{12}^+$ (open triangles)) as a function of irradiation time (Xe arc lamp, 475-nm long-pass filter). Experimental points for the parent and global fragment intensities are fitted according to eqs 1 and 2. The dashed lines were drawn to facilitate the reading.

studied, which allows to derive structures by means of DFT calculations. To rationalize the experimental results, in particular the decrease of the characteristic time scale for photodissociation when the size of the complex increases, we can then calculate bond dissociation energies (BDEs) and photon-absorption efficiencies using DFT and TD-DFT, respectively.

The most stable calculated structures obtained for $[FeC_{24}H_{12}]^+$, $[Fe(C_{24}H_{12})_2]^+$, and $[Fe_2(C_{24}H_{12})_2]^+$ at the BPW91/Lanl2dz level of theory, and their electronic states are reported in Figure 11. The BDEs obtained at the MPW1PW91/6-31+G(d,p)//BPW91/Lanl2DZ level are listed in Table 2.

In the structure of the ground state of $[FeC_{24}H_{12}]^+$, we found that the Fe atom interacts with an outer ring of coronene to form a ^{4}A complex (cf. Figure 11). This is in line with the conclusion drawn from DFT calculations on a series of model Fe-PAH complexes at the MPW1PW91/6-31+G(d,p) level of theory, considering two initial coordination sites for the iron atom (the inner or outer ring of the coronene molecule) and various spin states (doublet, quartet and sextet).[43] Five stable isomers for $[FeC_{24}H_{12}]^+$ π-complexes with Fe-PAH BDEs ranging from 1.0 to 2.6 eV were obtained. By consideration of the laser ablation conditions in our experiment ($\lambda = 266$ nm, fluence ≈ 0.04 J.cm^{-2}), only the most stable complexes are expected to survive in the "hot" initial plasma. In the present work, the BDE of the most stable $[FeC_{24}H_{12}]^+$ complex was calculated to be 2.6 eV (cf. Table 2), in agreement with the value previously estimated.[43] The most stable form for the $[Fe(C_{24}H_{12})_2]^+$ complex is commonly admitted to be a "sandwich structure" with the iron atom intercalated between two coronene molecules. After investigating the different possible sandwich isomers we found that in the most stable structure, the two coronene planes rotate away from each other to lead to a staggered structure in a quartet spin state (cf. Figure 11). This staggered geometry can be understood as it minimizes the electrostatic repulsion between the two coronene planes. Interestingly, similar structures were calculated for $[Fe(C_{24}H_{12})_2]^0$ and $[Fe(C_{24}H_{12})_2]^-$.[37] The$(C_{24}H_{12})$-$[FeC_{24}H_{12}]^+$ binding energy was estimated to be 1.7 eV (cf. Table 2). The lowest energy doublet spin state was found to lie 0.4 eV above the presented quartet spin state at the BPW91/Lanl2DZ level (and 1.0 eV at the MPW1PW91/6-31+G(d,p)//BPW91/Lanl2dz level). A more complete PES for $[Fe(C_{24}H_{12})_2]^+$ is under study.

For the $[Fe_2(C_{24}H_{12})_2]^+$ complex, a large number of a priori structural isomers are possible. The interaction site of a second Fe atom onto $[Fe(C_{24}H_{12})_2]^+$ is difficult to predict as the Fe−Fe interaction is expected to be of the same order of magnitude as the Fe-PAH interaction.[38] First calculations were performed on $[Fe_2(C_{24}H_{12})]^+$ complexes. We found that the two most stable structures, that lie within 0.04 eV, present an Fe−Fe interaction, whereas the lowest energy isomer with two separate Fe atoms on the surface of coronene, lies 1.17 eV above. This is in line with previous theoretical results showing that the ground-state geometry of $[Fe_2C_{24}H_{12}]^+$ is an iron dimer coordinated to the coronene surface.[39] Thus it seems reasonable to assume that the most stable structure for $[Fe_2(C_{24}H_{12})_2]^+$ presents an Fe−Fe interaction. The final sextet spin state optimized geometry is reported at the bottom of Figure 11. The exhaustive PES of $[Fe_2(C_{24}H_{12})_2]^+$ is under study. The most stable structure we calculated leads us to suggest that for multimetal-multiligand $[Fe_xPAH_y]$ complexes, a structure in which metal clusters are fully covered with PAH molecules (a so-called "rice-ball" structure) is likely to be preferred to a multiple-decker sandwich structure in which metal atoms are intercalated between single PAH molecules. This would be in line with the experimental results obtained by Kurikawa et al.[61] on multimetal-multiligand M_nBz_m transition metal-benzene complexes, showing that these adopt two types of structures according to the transition metal, a "rice-ball" structure when M is a late transition metal (Fe,

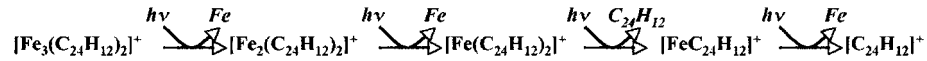

Figure 10. The photodissociation sequence for the $[Fe_x(C_{24}H_{12})_2]^+$ ($x = 1-3$) complexes as observed in the PIRENEA setup.

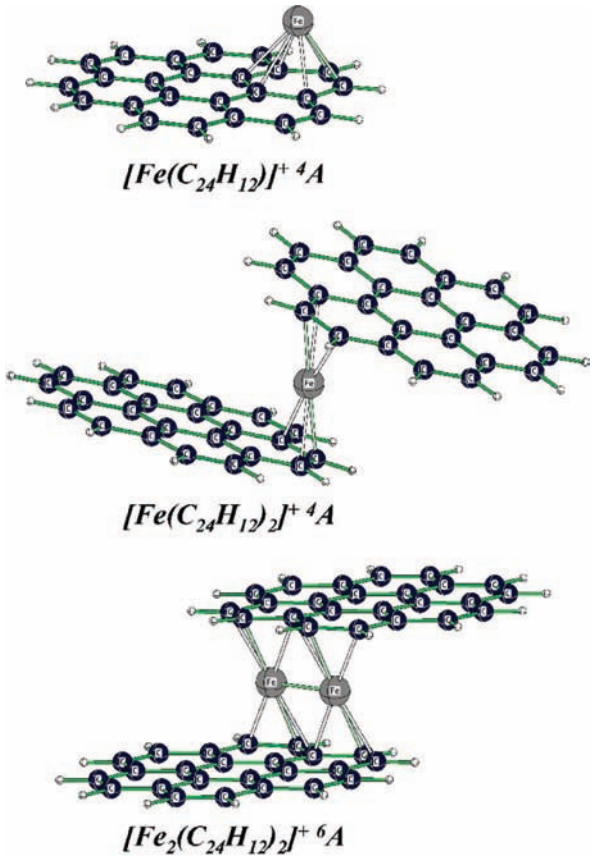

Figure 11. DFT calculations of the geometries and electronic states of the lowest energy minima determined for $[FeC_{24}H_{12}]^+$, $[Fe(C_{24}H_{12})_2]^+$, and $[Fe_2(C_{24}H_{12})_2]^+$ at the BPW91/Lanl2DZ level of theory.

Co, Ni) and a multiple-decker sandwich structure when M is an early transition metal (Sc−Mn).

This will have to be confirmed for $[Fe_3(C_{24}H_{12})_2]^+$, for which the number of possible a priori structures gets very large. After 200 ms of irradiation, the relative abundance of the $[Fe_2(C_{24}H_{12})_2]^+$ photofragment is 10% (Figure 9). This is comparable to the abundance of the $[Fe(C_{24}H_{12})_2]^+$ photofragment resulting from the loss of an iron atom from the $[Fe_2(C_{24}H_{12})_2]^+$ parent ion (Figure 7). This suggests that the Fe-$[Fe(C_{24}H_{12})_2]^+$ and Fe-$[Fe_2(C_{24}H_{12})_2]^+$ interactions are similar, again suggesting a metal-cluster configuration. Further experimental and theoretical studies are needed to investigate the structures of the $[Fe_3(C_{24}H_{12})_2]^+$ complex.

The differences in the dissociation time scale for the studied species could be due to variations of the BDEs but also of the heating efficiency in our experimental conditions. Under the soft continuous visible irradiation conditions used in our experiments, a progressive heating of the complexes is expected, thus leading to the lowest energy dissociation pathways. This is validated by our calculations for $[FeC_{24}H_{12}]^+$ and $[Fe(C_{24}H_{12})_2]^+$. The $[FeC_{24}H_{12}]^+$ dissociates into Fe and $C_{24}H_{12}^+$ as predicted by DFT calculations.[43] Similarly, the primary dissociation products of $[Fe(C_{24}H_{12})_2]^+$ are $[FeC_{24}H_{12}]^+$ and $C_{24}H_{12}$. The binding energy of the dissociating bond was calculated to be 1.7 eV (cf. Table 2). This is clearly the lowest energy dissociation channel (with respect to $[FeC_{24}H_{12}]$ and $C_{24}H_{12}^+$) given the calculated difference of 2 eV in the relative ionization potentials of $FeC_{24}H_{12}$ (5.08 eV) and $C_{24}H_{12}$ (7.05 eV).

The $[Fe(C_{24}H_{12})_2]^+$ complex was found to have a shorter characteristic dissociation time than $[FeC_{24}H_{12}]^+$. This decrease in the photostability can be understood by thermodynamic considerations. According to our calculations, the $[(C_{24}H_{12})$-$(FeC_{24}H_{12})^+]$ BDE (1.7 eV) is lower than that of $[FeC_{24}H_{12}]^+$ (2.6 eV, cf. Table 2). We cannot also exclude an increase of the heating efficiency, which depends on the photon flux and the absorption cross section in the visible.

The subsequent addition of Fe atoms leads to a further decrease of the characteristic dissociation time as observed for the $[Fe_2(C_{24}H_{12})_2]^+$ and $[Fe_3(C_{24}H_{12})_2]^+$ complexes (cf. Table 1). This cannot be understood by thermodynamic considerations. Indeed, as can be seen in Table 2, the Fe-$[Fe(C_{24}H_{12})_2^+]$ BDE (2.0 eV) was found to be close to the$(C_{24}H_{12})$-$[(C_{24}H_{12})Fe]^+$ BDE (1.7 eV), with a tendency for an increased stability with the number of Fe atoms. Further theoretical studies are ongoing to confirm this trend.[62] A clue to understand the increase of the photodissociation rate with the number of Fe atoms can be the increase of the density of electronic states reachable from the ground state by absorption of visible photons, thus enhancing the probability for an excitation energy with a strong oscillator strength in the visible and therefore the heating rate under visible irradiation. The discrete spectra of the excited states of $[FeC_{24}H_{12}]^+$, $[Fe(C_{24}H_{12})_2]^+$, and $[Fe_2(C_{24}H_{12})_2]^+$ were estimated at the TD-DFT level. They are reported in Figure 12. The results for the irradiation domain used in our experiment ([1.55−2.60 eV] or [475−800 nm]) are summarized in Table 2: the overall oscillator strength in this region is found to increase with the size of the cluster (cf. Table 2 and Figure 12). The effect is reinforced by the fact that $[Fe_2(C_{24}H_{12})_2]^+$ has a strong transition ($f = 0.16$) found at 2.14 eV (579 nm), where the transmission of the filter is maximum. Intense transitions are found at higher energy for the two smallest complexes: 2.62 eV (473 nm), which could still be in the filter transmission range, for $[Fe(C_{24}H_{12})_2]^+$ and 3.5 eV, out-of-the filter transmission, for $[FeC_{24}H_{12}]^+$ (Figure 12). From these theoretical results, we expect an increase of the heating efficiency with the number of Fe atoms in our experimental conditions. This is in line with the observed increase of the photodissociation rate.

To conclude this section, we emphasize that we managed to rationalize the experimental results with thermodynamic and excited-state calculations. These calculations have been performed on the most stable isomers. This choice appears then to be an a posteriori reasonable asumption.

Astrophysical Implications. Marty et al.[17] proposed that organometallic complexation involving Fe and PAHs can be responsible for the depletion of free PAHs to form aggregates, which could be related to VSGs, the carriers of the 25 μm IRAS emission band in mild UV-excited regions.[63] The recent work of Rapacioli et al.[12] and Berné et al.[13] shows that these VSGs are destroyed at the irradiated surface of the molecular clouds and liberate free PAHs in the gas phase. The experimental results presented here provide a nice scenario that fits with all the above studies. $[Fe_xPAH_y]$ complexes could be formed efficiently in molecular clouds according to Marty et al.[17] and get easily dissociated upon UV−vis irradiation to produce free PAHs (and Fe atoms/ions) according to our results. The similarity in the

TABLE 2: Calculated BDEs for the Dissociating Complexes, Obtained at the MPW1PW91/6-31+G(d,p)// BPW91/Lanl2DZ Level of Theory[a]

dissociation reaction	BDE	$E_{max}(f)$	$\langle E \rangle$	$\langle f \rangle$
$[FeC_{24}H_{12}]^+$ (^{4}A) → Fe (^{5}D) + $C_{24}H_{12}$ (^2A_u)	2.6	1.87 (0.01)	2.0	0.035
$[Fe_2(C_{24}H_{12})_2]^+$ (^{4}A) → $[(C_{24}H_{12})Fe]^+$ (^{4}A) + $C_{24}H_{12}$ (^1A_u)	1.7	2.55 (0.06)	2.3	0.21
$[Fe_2(C_{24}H_{12})_2]^+$ (^{6}A) → $[Fe_2(C_{24}H_{12})_2]^+$ (^{4}A) + Fe (^{5}D)	2.0	2.14 (0.16)	2.2	0.40

[a] The TD-DFT calculated excitation energies and oscillator strengths of the most intense transitions are reported ($E_{max}(f)$). The mean excitation energy ($\langle E \rangle$) and the integrated oscillator strength ($\langle f \rangle$) for the transitions in the [1.55−2.60 eV]([475−800 nm]) range of energy are also reported. These calculations were performed at the BPW91/Lanl2DZ level of theory. Energy values are expressed in electronvolts.

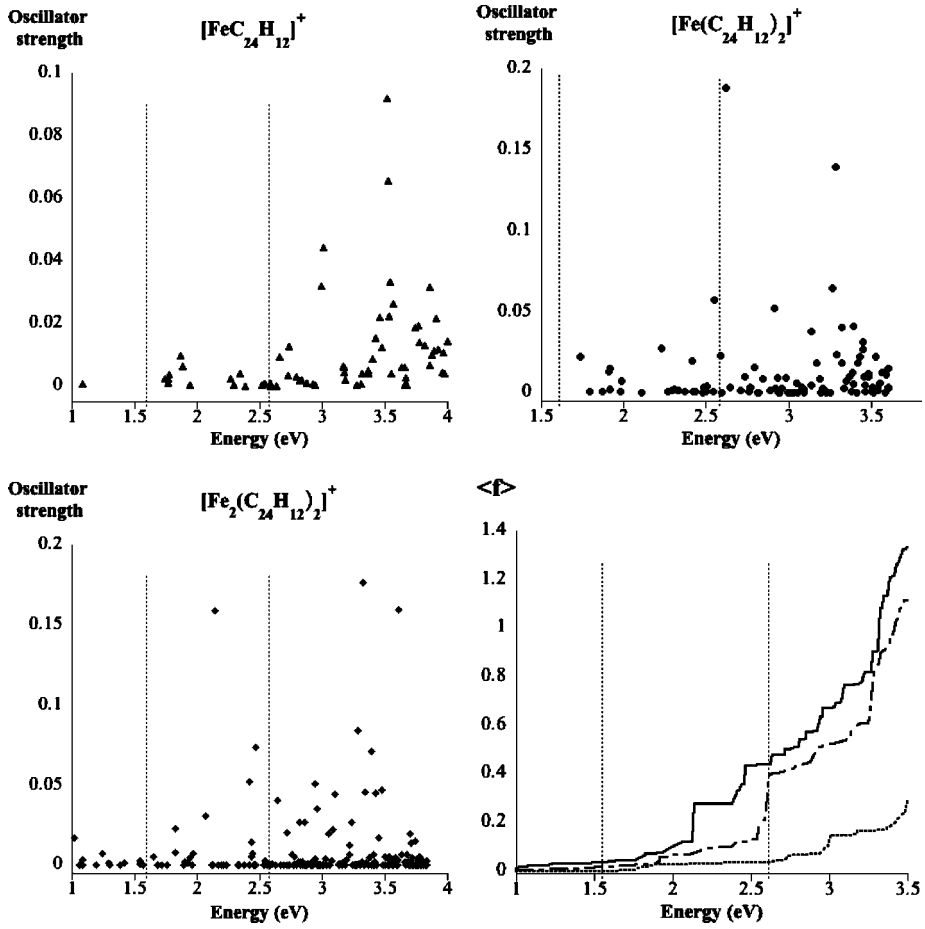

Figure 12. Electronic spectra of $[FeC_{24}H_{12}]^+$ (full triangles), $[Fe(C_{24}H_{12})_2]^+$ (full circles), and $[Fe_2(C_{24}H_{12})_2]^+$ (full diamonds) determined using TD-DFT at the BPW91/Lanl2DZ level of theory. The experimental energy range of the continuous irradiation (1.55−2.60 eV) is reported on each graph (domain between the dashed vertical lines). The right spectrum at the bottom represents the integrated oscillator strength $\langle f \rangle$ for $[FeC_{24}H_{12}]^+$ (dashed line), $[Fe(C_{24}H_{12})_2]^+$ (dot-dashed line), and $[Fe_2(C_{24}H_{12})_2]^+$ (plain line) as a function of energy.

stoichiometries of Fe and PAH units in the studied complexes is in agreement with the abundance constrains on these species in the ISM.[64] There are two points that have to be discussed concerning the implication of our results for astrochemistry, which are the relevance of (i) the species produced in the laboratory and (ii) the irradiation conditions.

As discussed in section 3.2, the complexes that are formed in our experimental conditions are likely to be the most stable. Experiments in collision-free conditions and at low temperatures are needed to conclude if these are the ones which would form under interstellar conditions. Still, considering that these complexes are submitted to a UV−visible radiation field with increasing intensity (and hardness) as they approach the border of the irradiated molecular clouds, it is likely that they will reach their most stable form before being dissociated.

The second concern is about the irradiation conditions. In interstellar conditions, each environment has specific local irradiation conditions, which are different from the laboratory conditions. Therefore the evolution of $[Fe_x(C_{24}H_{12})_y]^{+/0}$ complexes has to be modeled specifically. This was performed by Rapacioli et al.[15] for $[PAH]_n$ clusters in the NGC7023 reflection nebula. Such modeling requires the description of the absorption rate of UV−vis photons, the cooling rate by IR emission, and eventually by electronic fluorescence and the photodissociation rate. This is out of the scope of this paper. Still, we have used the kinetic Monte Carlo code[15,65] to describe the photophysics of $[FeC_{24}H_{12}]^+$ in our experimental conditions. The code provides the time evolution of the internal energy of the studied species as well as a description of the events: absorption of photons, IR emission, and dissociation. Previous studies on $C_{24}H_{12}^+$ have shown that this code can be successfully used to interpret the results of the photodissociation under irradiation with the Xenon arc lamp.[66] These studies show that a good description can only be obtained using time-dependent irradiation conditions. This can be interpreted as due to the

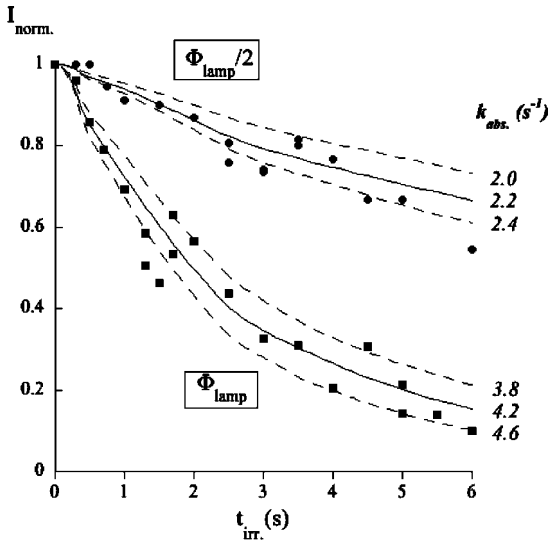

Figure 13. Normalized intensity of $[FeC_{24}H_{12}]^+$ as a function of the irradiation time with Xe arc lamp and 475-nm long-pass filter at full flux ϕ_{lamp} (full squares) and half flux $\phi_{lamp}/2$ (full circles). The lines represent the best fit resulting from the simulations, with a value of 10^{12} s^{-1} for A_d. The dispersion of the experimental points leads to several values for k_{abs} expressed in s^{-1} (values at the right).

expansion of the ion cloud under the action of collisions with background gas. This background pressure results from both buffer gas injection and desorption from surfaces during lamp irradiation.

The mean absorption rate of photons k_{abs} in s^{-1} can be expressed as follows

$$k_{abs} = \int_{475nm}^{800nm} \sigma_{abs}(\lambda)\phi(\lambda)d\lambda \quad (8)$$

with $\sigma_{abs}(\lambda)$ the absorption cross section and $\phi(\lambda)$ the flux of photons from the lamp. The mean excitation energy in the [475−800] nm range was found to be 2.0 eV with a mean oscillator strength of 0.035 (cf. Table 2), so we assumed to simplify the calculations that there is only one absorption channel at 2 eV. In our calculations, k_{abs} is a free parameter since it is difficult to access to the absolute photon flux seen by the ions in the cell. To further constrain k_{abs}, we have run a second measurement in which the photon flux was reduced by 50% using a neutral density filter. As already mentionned in the text, the energy which is absorbed in an electronic excited state is assumed to be rapidly converted into vibrational energy in the ground state, as generally observed for PAHs.[67] For the cooling, we only consider the emission of IR photons. Electronic emission could also play a role in the cooling rate, but we did not try to include this process for which we lack quantitative data. The consequences will be discussed below.

The rate of spontaneous emission for a ν_i IR mode in the $v_i \rightarrow v_i-1$ transition is given by

$$k_{IR}^{v_i,v_i-1}(\nu_i) = A_i^{v_i,v_i-1}P_i^{v_i} \quad (9)$$

where $A_i^{v_i,v_i-1}$ is the Einstein coefficient ($A_i^{v_i,v_i-1} = v_i A_i^{1,0}$ in the harmonic case) and $P_i^{v_i}$ the probability to find the system in the level v_i of the ν_i mode. In the statistical approach, the probability can be calculated as follows

$$P_i^{v_i} = \frac{\rho^*(U - v_i h\nu_i)}{\rho(U)} \quad (10)$$

where $\rho(U)$ is the total density of states at energy U and ρ^* is the density of states excluding the emitting mode ν_i. The harmonic vibrational frequencies and the associated Einstein coefficients for $[FeC_{24}H_{12}]^+$ are taken from Simon and Joblin.[43]

Finally the dissociation rate k_d expressed in s^{-1} is given by

$$k_d = A_d \frac{\rho(U - E_d)}{\rho(U)} \quad (11)$$

with A_d the pre-exponential factor and E_d the dissociation energy,[60] similar to the factors A and E_a in the Arrhenius law that provides the canonical (or high-pressure) limit. A_d is a free parameter in our calculations. E_d was taken as 2.6 eV, the BDE we calculated for $Fe-C_{24}H_{12}^+$ (cf. Table 2).

By adjusting the results of the simulations to the experimental data obtained for the two values of the incident flux (cf. Figure 13), the best value for A_d was found to be 10^{12} s^{-1} and the values for k_{abs} to be 4.2 ± 0.4 and 2.2 ± 0.2 s^{-1}. In the Arrhenius law, the value of the pre-exponential factor is often found to be of the order of 10^{13} s^{-1}, which corresponds to a typical vibrational frequency of 1000 cm^{-1}. The Fe-PAH dissociating bond is

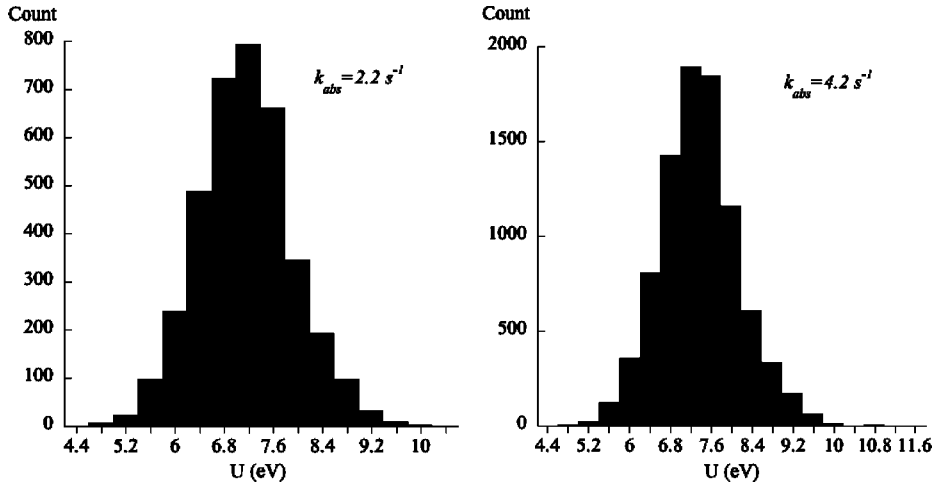

Figure 14. Distribution of the internal energy in the dissociating $[FeC_{24}H_{12}]^+$ complex using the kinetic Monte Carlo code with a value of 10^{12} s^{-1} for A_d and with values of 2.2 (left) and 4.2 (right) s^{-1} for k_{abs}.

expected at lower frequency (~400 down to 100 cm^{-1}), which is therefore consistent with the value of 10^{12} s^{-1} we derived. The variation of the derived heating rate k_{abs} (4.2 ± 0.4 down to 2.2 ± 0.2 s^{-1}) is consistent with the variation of the photon flux (ϕ down to $\phi/2$). The satisfactory fit obtained for the dissociation yield, which results from the competition between the cooling rate and the dissociating rate, implies that this cooling rate is properly described and thus excludes a significant contribution from electronic fluorescence. From the output of the kinetic Monte Carlo model, we can build the histogram of the internal energy at the time of dissociation. For an A_d value of 10^{12} s^{-1} and $k_{abs} = 4.2$ or 2.2 s^{-1}, the internal energy of $[FeC_{24}H_{12}]^+$ complexes at dissociation lies between 5.2 and 9.2 eV, as can be seen in Figure 14. The low-energy side of the distribution reflects the increased probability of dissociation when the internal energy increases. The high-energy side reflects the decreased probability that the ion stores ~7 eV of internal energy without being dissociated. The distributions of energies displayed in Figure 14 also show that the dissociation threshold for $[FeC_{24}H_{12}]^+$ is ~5 eV. These complexes are thus expected to be easily destroyed in the ISM by absorption of a single UV photon.

For complexes containing a large number of PAH units, starting with two such as in $[Fe(C_{24}H_{12})_2]^+$, we expect the dissociation rate to be smaller for a given internal energy due to the increase number of vibrational modes leading to a lower probability to localize the energy E_d in the dissociating bond. At the same time, the value of E_d is smaller (1.7 eV compared to 2.6 eV), which increases significantly the probability of dissociation. Besides, the UV electronic absorption cross section is expected to be larger in these systems. For PAHs, the UV cross section, which is due to $\pi \rightarrow \pi^*$ and $\sigma \rightarrow \sigma^*$ transitions is found to increase with the number of C atoms.[68,69] For an aggregate of PAHs, we expect a similar scaling although it has not been calculated. The inclusion of Fe atoms is expected to lead to stronger perturbations of the π cloud, and therefore the scaling factor would be more affected. Still, we expect a global trend of increasing the UV cross section with the number of C atoms. For such large systems, multiple photon events can become important. For instance, Rapacioli et al. have shown that such a process accounts for the dissociation of $(C_{24}H_{12})_{13}$ clusters in NGC7023.[15] In the case of $[Fe_x(C_{24}H_{12})_y]^{+/0}$ complexes, this process could even be efficient under visible irradiation due to the opening of numerous electronic transitions in this range.

Finally, compared to the work by Rapacioli et al.,[15] we find that the presence of Fe atoms in the coronene clusters increases the stability of the aggregate. For instance, the BDE of the coronene dimer is calculated to be ~1 eV for the neutral dimer$(C_{24}H_{12})_2$[70] and ~1.3 eV for the positively charged dimer $[(C_{24}H_{12})_2]^+$.[71] In this paper, the BDEs were found to be 1.7 eV for $[Fe(C_{24}H_{12})_2]^+$ and 2.0 eV for $[Fe_2(C_{24}H_{12})_2]^+$. This implies that the presence of Fe atoms in the ionized aggregates further increases the stability compared to the homogeneous clusters. This is expected to increase the lifetime of these species in the ISM. A model taking into account formation and destruction processes would be necessary to determine the relative lifetimes of these various complexes in interstellar conditions.

Conclusion and Future Work

The work presented in this paper is a pioneering experimental study which aims at exploring the presence of iron atoms in interstellar carbonaceous VSGs, which is plausible given the observational constrains. For the first time, a series of $[Fe_x(C_{24}H_{12})_y]^+$ $(x,y) = ((1,1)$ and $(1-3, 2))$ complexes are isolated under interstellar conditions in the PIRENEA setup, a cold ion trap dedicated to astrochemistry. Each complex is irradiated with low-energy continuous visible irradiation and gets photodissociated, leading to the sequential loss of Fe atoms and PAH units. The carbonaceous skeleton of PAHs is not affected. This makes these clusters good candidates for interstellar VSGs, which have been proposed to liberate free PAHs in the gas phase upon UV irradiation. The presence of iron inside these clusters confers them with new properties such as an increased stability and a larger absorption cross section in the visible range. These first results encourage further spectroscopic studies on these species including IR spectroscopy, which provides a more direct comparison with astronomical data. The detection of these species in space would open the opportunity for a new chemistry, which still has to be explored, as complexes of Fe with large PAHs are expected to act as efficient platforms for catalytic gas-phase chemistry.[31]

Acknowledgment. The authors would like to thank the technical team of PIRENEA (M. Armengaud, P. Frabel, L. Noguès, and A. Bonnamy), D. Toublanc for his support with the kinetic Monte Carlo model, and C. Nayral for kindly providing silica nanoparticles. This work was supported by the French National Program, Physique et Chimie du Milieu Interstellaire, which is gratefully acknowledged. DFT calculations were performed at the CALMIP supercomputing facility of Université Toulouse 3. Finally, the authors thank the reviewers for their comments that helped to improve the manuscript.

References and Notes

(1) Léger, A.; Puget, J. L. *Astronom. Astrophys.* **1984**, *137*, L5–L8.
(2) Allamandola, L. J.; Tielens, A. G. G. M.; Barker, J. R. *Astrophys. J. Lett.* **1985**, *290*, L25–L28.
(3) Bohme, D. K. *Chem. Rev.* **1992**, *92*, 1487–1508.
(4) Cherchneff, I.; Barker, J. R.; Tielens, A. G. G. M. *Astrophys. J.* **1992**, *401*, 269–287.
(5) Cernicharo, J.; Heras, A. M.; Tielens, A. G. G. M.; Pardo, J. R.; Herpin, F.; Guélin, M.; Waters, L. B. F. M. *Astrophys. J. Lett.* **2001**, *546*, L123–L126.
(6) Sloan, G. C.; Jura, M.; Duley, W. W.; Kraemer, K. E.; Bernard-Salas, J.; Forrest, W. J.; Sargent, B.; Li, A.; Barry, D. J.; Bohac, C. J.; Watson, D. M.; Houck, J. R. *Astrophys. J.* **2007**, *664*, 1144–1153.
(7) Joblin, C.; Szczerba, R.; Berné, O.; Szyszka, C. *Astron. Astrophys.* **2008**, *490*, 189–196.
(8) Tielens, A. G. G. M. *Ann. Rev. Astron. Astrophys.* **2008**, *46*, 289–337.
(9) Jones, A. P.; Tielens, A. G. G. M.; Hollenbach, D. J. *Astrophys. J.* **1996**, *469*, 740–764.
(10) Boulanger, F.; Falgarone, E.; Puget, J. L.; Helou, G. *Astrophys. J.* **1990**, *364*, 136–145.
(11) Bernard, J. P.; Boulanger, F.; Puget, J. L. *Astronom. Astrophys.* **1993**, *277*, 609–622.
(12) Rapacioli, M.; Joblin, C.; Boissel, P. *Astronom. Astrophys.* **2005**, *429*, 193–204.
(13) Berné, O.; Joblin, C.; Deville, Y.; Smith, J. D.; Rapacioli, M.; Bernard, J. P.; Thomas, J.; Reach, W.; Abergel, A. *Astronom. Astrophys.* **2007**, *469*, 575–586.
(14) Draine, B. T.; Li, A. *Astrophys. J.* **2001**, *551*, 807–824.
(15) Rapacioli, M.; Calvo, F.; Joblin, C.; Parneix, P.; Toublanc, D.; Spiegelman, F. *Astronom. Astrophys.* **2006**, *460*, 519–531.
(16) Schmidt, M.; Masson, A.; Bréchignac, C. *Int. J. Mass Spectrom.* **2006**, *252*, 173–179.
(17) Marty, P.; Serra, G.; Chaudret, B.; Ristorcelli, I. *Astronom. Astrophys.* **1994**, *282*, 916–923.
(18) Serra, G.; Chaudret, B.; Saillard, Y.; Le Beuze, A.; Rabaa, H.; Ristorcelli, I.; Klotz, A. *Astronom. Astrophys.* **1992**, *260*, 489–493.
(19) Chaudret, B.; Le Beuze, A.; Rabaa, H.; Saillard, Y.; Serra, G. *New J. Chem.* **1991**, *15*, 791.
(20) Klotz, A.; Marty, P.; Boissel, P.; Serra, G.; Chaudret, B.; Daudey, J. P. *Astronom. Astrophys.* **1995**, *304*, 520–530.

(21) Weingartner, J. C.; Draine, B. T. *Astrophys. J.* **1999**, *517*, 292–298.
(22) Rodríguez, M. *Astronom. Astrophys.* **2002**, *389*, 556–567.
(23) Whittet, D. C. B. *Dust in the Galactic Environment*, 2nd ed.; Institute of Physics: Bristol, 2003.
(24) Rodríguez, M.; Rubin, R. H. *Astrophys. J.* **2005**, *626*, 900–908.
(25) Miller, A.; Lauroesch, J. T.; Sofia, U. J.; Cartledge, S. I. B.; Meyer, D. M. *Astrophys. J.* **2007**, *659*, 441–446.
(26) Cecchi-Pestellini, C.; Malloci, G.; Mulas, G.; Joblin, C.; Williams, D. A. *Astronom. Astrophys.* **2008**, *486*, L25–L29.
(27) Boissel, P. *Astronom. Astrophys.* **1994**, *285*, L33–L36.
(28) Szczepanski, J.; Wang, H.; Vala, M.; Tielens, A. G. G. M.; Eyler, J. R.; Oomens, J. *Astrophys. J.* **2006**, *646*, 666–680.
(29) Pozniak, B. P.; Dunbar, R. C. *J. Am. Chem. Soc.* **1997**, *119*, 10439–10445.
(30) Caraiman, D.; Koyanagi, G. K.; Scott, L. T.; Preda, D. V.; Bohme, D. K. *J. Am. Chem. Soc.* **2001**, *123*, 8573–8582.
(31) Caraiman, D.; Bohme, D. K. *Int. J. Mass Spectrom.* **2003**, *223*, 411–425.
(32) Ayers, T. M.; Westlake, B. C.; Duncan, M. A. *J. Phys. Chem. A* **2004**, *108*, 9805–9813.
(33) Buchanan, J. W.; Reddic, J. E.; Grieves, G. A.; Duncan, M. A. *J. Phys. Chem. A* **1998**, *102*, 6390–6394.
(34) Foster, N. R.; Grieves, G. A.; Buchanan, J. W.; Flynn, N. D.; Duncan, M. A. *J. Phys. Chem. A* **2000**, *104*, 11055–11062.
(35) Duncan, M. A.; Knight, A. M.; Negishi, Y.; Nagao, S.; Judai, K.; Nakajima, A.; Kaya, K. *J. Phys. Chem. A* **2001**, *105*, 10093–10097.
(36) Foster, N. R.; Buchanan, J. W.; Flynn, N. D.; Duncan, M. A. *Chem. Phys. Lett.* **2001**, *341*, 476–482.
(37) Li, X.; Eustis, S.; Bowen, K. H.; Kandalam, A. K.; Jena, P. *J. Chem. Phys.* **2008**, *129*, 074313.
(38) Scott, A. C.; Buchanan, J. W.; Flynn, N. D.; Duncan, M. A. *Int. J. Mass Spectrom.* **2007**, *266*, 149–155.
(39) Senapati, L.; Nayak, S. K.; Rao, B. K.; Jena, P. *J. Chem. Phys.* **2003**, *118*, 8671–8680.
(40) Simon, A.; Joblin, C.; Polfer, N.; Oomens, J. *J. Phys. Chem. A* **2008**, *112*, 8551–8560.
(41) Klippenstein, S. J.; Yang, C. N. *Int. J. Mass Spectrom.* **2000**, *201*, 253–267.
(42) Philpott, M. R.; Kawazoe, Y. *Chem. Phys.* **2007**, *342*, 223–235.
(43) Simon, A.; Joblin, C. *J. Phys. Chem. A* **2007**, *111*, 9745–9755.
(44) Joblin, C.; Pech, C.; Armengaud, M.; Frabel, P.; Boissel, P. A piece of interstellar medium in the laboratory: the PIRENEA experiment. *EAS Pubs. Ser.* **2002**, 73–77.
(45) Marshall, A. G.; Schweikhard, L. *Int. J. Mass Spectrom. Ion Process.* **1992**, *118*, 37.
(46) Guan, S.; Marshall, A. G. *Int. J. Mass Spectrom. Ion Process.* **1996**, *157−158*, 5.
(47) Becke, A. D. *Phys. Rev. A* **1988**, *38*, 3098.
(48) Perdew, J. P.; Wang, Y. *Phys. Rev. B* **1992**, *45*, 13244–13249.
(49) Hay, P. J.; Wadt, W. R. *J. Chem. Phys.* **1985**, *82*, 270–283.
(50) Gutsev, G. L.; Bauschlicher, C. W. *J. Phys. Chem. A* **2003**, *107*, 7013–7023.
(51) Yu, S. Q.; Chen, S. G.; Zhang, W. W.; Yu, L. H.; Yin, Y. S. *Chem. Phys. Lett.* **2007**, *446*, 217–222.
(52) Adamo, C.; Barone, V. *J. Chem. Phys.* **1998**, *108*, 664–675.
(53) Porezag, D.; Frauenheim, T.; Köhler, T.; Seifert, G.; Kaschner, R. *Phys. Rev. B* **1995**, *51*, 12947–12957.
(54) Seifert, G.; Porezag, D.; Frauenheim, T. *Int. J. Quantum Chem.* **1996**, 185–192.
(55) Elstner, M.; Porezag, D.; Jungnickel, G.; Elsner, J.; Haugk, M.; Frauenheim, T.; Suhai, S.; Seifert, G. *Phys. Rev. B* **1998**, *58*, 7260–7268.
(56) Koster, A.; Geutner, G.; Goursot, A.; Heine, T.; Vela, A.; Patchkovskii, S.; Salahub, D. *Code Demon*; Technical Report, 2004.
(57) Runge, E.; Gross, E. K. U. *Phys. Rev. Lett.* **1984**, *52*, 997.
(58) Frisch, M. J.; Trucks, G. W.; Schlegel, H. B.; Scuseria, G. E.; Robb, M. A.; Cheeseman, J. R.; Montgomery, J. A., Jr.; Vreven, T.; Kudin, K. N.; Burant, J. C.; Millam, J. M.; Iyengar, S. S.; Tomasi, J.; Barone, V.; Mennucci, B.; Cossi, M.; Scalmani, G.; Rega, N.; Petersson, G. A.; Nakatsuji, H.; Hada, M.; Ehara, M.; Toyota, K.; Fukuda, R.; Hasegawa, J.; Ishida, M.; Nakajima, T.; Honda, Y.; Kitao, O.; Nakai, H.; Klene, M.; Li, X.; Knox, J. E.; Hratchian, H. P.; Cross, J. B.; Bakken, V.; Adamo, C.; Jaramillo, J.; Gomperts, R.; Stratmann, R. E.; Yazyev, O.; Austin, A. J.; Cammi, R.; Pomelli, C.; Ochterski, J. W.; Ayala, P. Y.; Morokuma, K.; Voth, G. A.; Salvador, P.; Dannenberg, J. J.; Zakrzewski, V. G.; Dapprich, S.; Daniels, A. D.; Strain, M. C.; Farkas, O.; Malick, D. K.; Rabuck, A. D.; Raghavachari, K.; Foresman, J. B.; Ortiz, J. V.; Cui, Q.; Baboul, A. G.; Clifford, S.; Cioslowski, J.; Stefanov, B. B.; Liu, G.; Liashenko, A.; Piskorz, P.; Komaromi, I.; Martin, R. L.; Fox, D. J.; Keith, T.; Al-Laham, M. A.; Peng, C. Y.; Nanayakkara, A.; Challacombe, M.; Gill, P. M. W.; Johnson, B.; Chen, W.; Wong, M. W.; Gonzalez, C.; Pople, J. A. *Gaussian 03*, revision C.02; Gaussian, Inc.: Wallingford, CT, 2004.
(59) El Hawi, N.; Nayral, C.; Delpech, F.; Chaudret, B. In preparation.
(60) Boissel, P.; de Parseval, P.; Marty, P.; Lefèvre, G. *J. Chem. Phys.* **1997**, *106*, 4973–4984.
(61) Kurikawa, T.; Takeda, H.; Hirano, M.; Judai, K.; Arita, T.; Nagao, S.; Nakajima, A.; Kaya, K. *Organometallics* **1999**, *18*, 1430–1438.
(62) Simon, A.; Joblin, C.; Patzer, B.; Chang, C. In preparation.
(63) Désert, F.-X.; Boulanger, F.; Puget, J. L. *Astronom. Astrophys.* **1990**, *237*, 215–236.
(64) Joblin, C.; Berné, O.; Simon, A. Laboratory studies of polycyclic aromatic hydrocarbons: the search for interstellar candidates *Cosmic Dust - Near and Far, ASP Conf. Series* **2009**.
(65) Joblin, C.; Toublanc, D.; Boissel, P.; Tielens, A. G. G. M. *Mol. Phys.* **2002**, *100*, 3595–3600.
(66) Joblin, C.; Toublanc, D.; Pech, C.; Toublanc, D.; Boissel, P.; Armengaud, M.; Frabel, P. In preparation.
(67) Léger, A.; D'Hendecourt, L.; Defourneau, D. *Astronom. Astrophys.* **1989**, *216*, 148–164.
(68) Joblin, C.; Léger, A.; Martin, P. *Astrophys. J. Lett.* **1992**, *393*, L79–L82.
(69) Malloci, G.; Mulas, G.; Joblin, C. *Astronom. Astrophys.* **2004**, *426*, 105–117.
(70) Rapacioli, M.; Calvo, F.; Spiegelman, F.; Joblin, C.; Wales, D. J. *J. Phys. Chem. A* **2005**, *109*, 2487–2497.
(71) Rapacioli, M.; Spiegelman, F. *Eur. Phys. J. D.* **2009**, DOI: 10.1140/epjd/e2008-00280-2 (http://adsabs.harvard.edu/abs/2009EPJD..tmp...39R).

JP8099785